

# Growth-mode investigation of epitaxial EuS on InAs(100)

Cite as: AIP Advances **9**, 035016 (2019); <https://doi.org/10.1063/1.5080123>

Submitted: 05 November 2018 . Accepted: 20 December 2018 . Published Online: 13 March 2019

Norman V. Blümel , Alexander Goschew, Yasser A. Shokr, and Paul Fumagalli 

## COLLECTIONS

Paper published as part of the special topic on [2019 Joint MMM-Intermag Conference](#)



View Online



Export Citation



CrossMark

## ARTICLES YOU MAY BE INTERESTED IN

[Magnetic properties of “thick” glass-coated Fe-rich microwires](#)

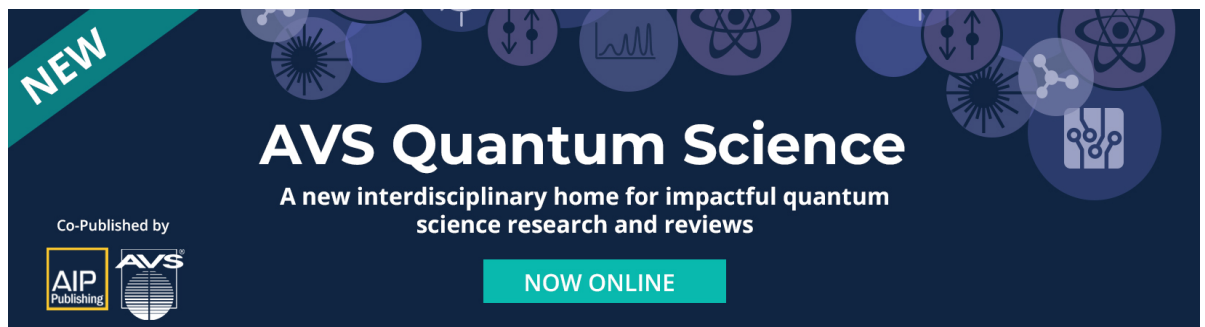
AIP Advances **9**, 035017 (2019); <https://doi.org/10.1063/1.5077009>

[Characterization of multilayered structures by swept-frequency eddy current testing](#)

AIP Advances **9**, 035009 (2019); <https://doi.org/10.1063/1.5079959>

[3D structure design of magnetic ferrite cores using gelcasting and pressure-less sintering process](#)

AIP Advances **9**, 035006 (2019); <https://doi.org/10.1063/1.5080008>





**NEW**

## AVS Quantum Science

A new interdisciplinary home for impactful quantum science research and reviews

Co-Published by



**NOW ONLINE**

# Growth-mode investigation of epitaxial EuS on InAs(100)

Cite as: AIP Advances 9, 035016 (2019); doi: 10.1063/1.5080123  
Presented: 17 January 2019 • Submitted: 5 November 2018 •  
Accepted: 20 December 2018 • Published Online: 13 March 2019



Norman V. Blümel,<sup>1,a)</sup> Alexander Goschew,<sup>1</sup> Yasser A. Shokr,<sup>1,2</sup> and Paul Fumagalli<sup>1</sup>

## AFFILIATIONS

<sup>1</sup>Department of Physics, Freie Universität Berlin, Berlin 14195, Germany

<sup>2</sup>Faculty of Science, Department of Physics, Helwan University, 17119 Cairo, Egypt

**Note:** This paper was presented at the 2019 Joint MMM-Intermag Conference.

<sup>a)</sup>[norman.vietvien.bluemel@gmail.com](mailto:norman.vietvien.bluemel@gmail.com)

## ABSTRACT

A persistent challenge in the field of spintronics is the search for suitable materials that enable the circumvention of the impedance mismatch preventing efficient spin-injection from metallic ferromagnetic conductors into semiconductors. One promising material is europium sulfide (EuS), a ferromagnetic semiconductor below the Curie temperature of 16.5 K. Investigation and optimization of the conditions required for high-quality growth of epitaxial EuS films on suitable substrates are thus of particular interest for the creation of efficient devices. We present the results of a growth-mode study employing atomic force microscopy and spot-profile analysis low-energy electron diffraction (SPA-LEED) of epitaxial EuS thin films deposited by electron-beam evaporation on InAs(100) substrates with varying combinations of, respectively, growth and annealing temperatures,  $T_g$  and  $T_a$ , from room temperature to 400 °C. We observed Stranski-Krastanov-like growth featuring low-roughness surfaces with root mean square values between 0.4 – 0.9 nm for all temperature combinations. An increased tendency for nucleation into grains and islands was observed for higher  $T_a$  from 300 – 400 °C. The corresponding nucleation mode, defined by varying degrees of 2D and 3D nucleation, was dependent on  $T_g$ . A 2D island growth mode was observed for  $T_g = 150$  °C and  $T_a = 400$  °C featuring a sharp and bright SPA-LEED pattern. This suggests the formation of a highly ordered, smooth surface for these growth conditions thereby providing a good starting point for optimization attempts for potential future devices.

© 2019 Author(s). All article content, except where otherwise noted, is licensed under a Creative Commons Attribution (CC BY) license (<http://creativecommons.org/licenses/by/4.0/>). <https://doi.org/10.1063/1.5080123>

## I. INTRODUCTION

The interest in the research field of spintronics is still unbroken and has been such for several decades.<sup>1–3</sup> It aims to combine the electronic and magnetic properties of charge carriers to construct new electronic devices. Among the expected advantages of such devices are faster data processing and more substantial magnetic storage capabilities.<sup>4,5</sup> The ideal spintronic device would thus be a magnetic semiconductor with a Curie temperature ( $T_C$ ) far above room temperature (RT).

Europium sulfide (EuS) is such a magnetic semiconductor with a very high magnetic moment of  $7 \mu_B$  per Eu atom, coming from a highly localized, half-filled 4f shell.<sup>6</sup> The bandgap energy is 1.65 eV and has been shown to be tunable by quantum-confinement effects.<sup>7</sup>

The current main drawback of EuS is its low  $T_C$  of 16.5 K. However, a higher  $T_C$  has been reported for lattice contracted EuS

due to growth dislocations<sup>8</sup> or high pressure.<sup>9</sup> Additionally, it was found that  $T_C$  of EuS could be increased significantly to 180 K in EuS nanoparticles embedded in a Co matrix<sup>10</sup> or even above RT in conjunction with Co or Ni in multilayer structures.<sup>11–13</sup>

Apart from the ferromagnetic properties, the film quality of the EuS layers will also play a crucial role in future devices. Earlier studies of epitaxial growth of EuS were conducted on different materials such as Si, PbS and BaF<sub>2</sub> with differing outcomes.<sup>14–16</sup> Our attempts focused on the choice of the two semiconductors InP(100) and InAs(100) as substrates because of the minimal lattice mismatch of only 1.5 %. For both substrates, epitaxial growth of EuS was confirmed but with varying film qualities. Generally, films grown on InAs show higher quality.<sup>17</sup> Therefore, this paper will focus on optimizing and understanding the epitaxial growth of EuS films on InAs through study of their growth mode and surface quality for different growth parameters.

## II. EXPERIMENTAL DETAILS

All samples were prepared by e-beam evaporation of EuS powder of 99.9 % purity from a tungsten crucible onto commercially available 1 cm  $\times$  1 cm InAs(100) substrates in an ultrahigh-vacuum chamber with a base pressure of  $2 \times 10^{-10}$  mbar.

Before evaporation, the InAs substrates were sputtered with argon gas (1 kV) for one hour and then annealed at 300  $^{\circ}$ C for 30 minutes to remove any surface contaminants. Later, the purity and crystallinity of the substrate surface were confirmed by Auger electron spectroscopy (AES) and spot-profile analysis low-energy electron diffraction (SPA-LEED) by detecting the typical InAs  $c(8 \times 2)/(4 \times 2)$  surface reconstruction. In cases where AES or LEED identified remaining contamination of the substrate, the cleaning procedure was repeated.

During film growth, the film thickness was monitored by an appropriately calibrated quartz microbalance and the substrate temperature was regulated through indirect heating from the back of the sample with a controllable heater, integrated into the sample holder. After reaching the desired film thickness, the samples were annealed at the chosen temperatures for an additional 30 minutes and then checked for surface contaminations employing AES.

For this work, eight samples were prepared in the above manner with a EuS film thickness of 4 nm at varying combinations of growth and annealing temperatures ranging from RT up to 400  $^{\circ}$ C.

The experimental methods employed for the surface characterization of the deposited films were SPA-LEED and atomic force microscopy (AFM).

## III. EXPERIMENTAL RESULTS

An essential parameter for the creation of potential future devices based on epitaxially grown EuS films on InAs is the dependence of film roughness and crystallinity, i.e., the film quality, on the growth conditions such as the growth and annealing temperatures  $T_g$  and  $T_a$ , respectively. In general, films featuring crystalline surfaces of low roughness are desirable to ensure optimal device efficiency by providing a potentially high interface quality with other device components or electrical contacts. In this section, we therefore present the results of our investigation of the film roughness and crystallinity for different combinations of  $T_g$  and  $T_a$ .

Figure 1 shows SPA-LEED patterns (left row) and corresponding AFM images (right row) of four of the eight films investigated. All SPA-LEED patterns were recorded using an electron beam energy of 67.5 eV, corresponding to the 4<sup>th</sup> in-phase condition of the (00)-spot of the ideal EuS lattice. They are depicted on a logarithmic intensity scale. The AFM images each show the topography of a 500 nm  $\times$  500 nm sized area on the EuS film surface. The image resolution varied between sampling sizes of 1 - 3 nm. Both, SPA-LEED patterns and AFM images were recorded at the center of each sample to enable the comparison of the results obtained with the two locally constrained techniques.

The SPA-LEED examination of all investigated samples showed a simple  $1 \times 1$  LEED pattern as expected from an unreconstructed NaCl-type face-centered cubic (fcc) lattice like EuS mirroring our earlier studies of EuS grown on InAs(100).<sup>17</sup> This confirms successful epitaxial growth for all chosen combinations of  $T_g$  and  $T_a$ . In SPA-LEED investigations both, the intensities and widths of the

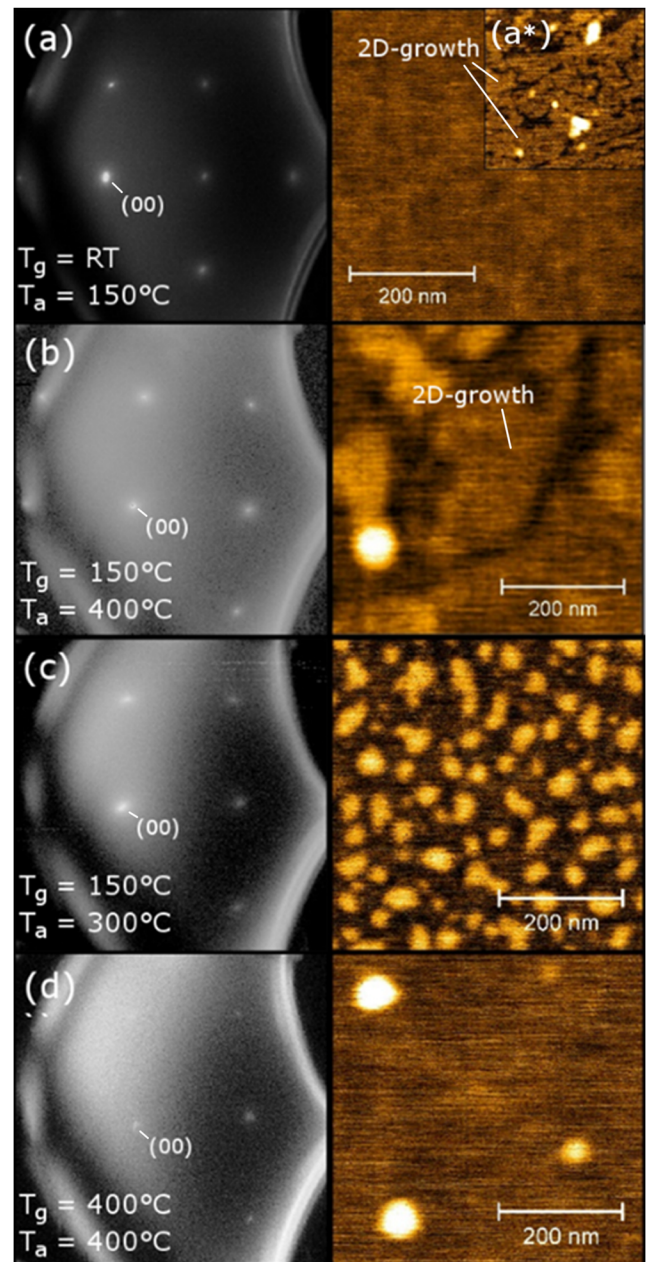


**FIG. 1.** SPA-LEED patterns (left row) with logarithmic intensity scaling and (00)-spots marked and corresponding AFM images (right row) of EuS thin films of 4 nm thickness on InAs(100) with different combinations of growth parameters  $T_g$  and  $T_a$  indicated in (a)-(d). Both, SPA-LEED and AFM investigation reveal a clear dependence of the surface quality on the chosen growth parameters with Stranski-Krastanov-like growth featuring different degrees of 2D and 3D nucleation. (a\*) shows a secondary topography found on the corresponding sample.

recorded diffraction spots are highly sensitive to the local surface roughness, i.e., the topography variation below the transfer width (approx. 100 nm<sup>18</sup>) of the SPA-LEED setup.<sup>19,20</sup> Determination of the quality factor  $Q_{hk} = I_{hk}/FWHM_{hk}$ , i.e., the ratio between intensity

**TABLE I.** Growth and annealing temperature dependence of EuS film<sup>a</sup> SPA-LEED quality factors.

$T_g$	$Q_{00}$		$Q_{00}$		$Q_{00}$	
	$T_a = 150\text{ }^\circ\text{C}$	Cat.	$T_a = 300\text{ }^\circ\text{C}$	Cat.	$T_a = 400\text{ }^\circ\text{C}$	Cat.
RT	-3.4(3) <sup>b</sup>	1/2	7.4(5)	2	0.3(1)	1
150 °C	-		0.6(1)	3	6.8(4)	2
300 °C	-		0.6(1)	1	0.9(2)	3
400 °C	-		-		1.2(4)	1

<sup>a</sup>All samples were deposited with a film thickness of 4 nm.

<sup>b</sup>This sample showed both topographies of category 1 and 2, the tabulated Q factor is presumed to correspond to the latter.

$I$  and full-width-half-maximum  $FWHM$  of a specific diffraction spot with Miller indices  $(hk)$ , therefore constitutes a semi-quantitative approach to compare the surface quality of different samples.

Here, the (00) diffraction spots were analyzed as the diffraction patterns were recorded at their in-phase condition. The resulting  $Q_{00}$ -factors (Table I) are thus higher for sample topographies that are closer to an ideal, smooth surface, defined by a diffraction pattern only affected by instrumental broadening.<sup>21</sup> Spot intensities and widths were obtained by averaging fit parameters of Lorentzian-Gaussian fits of vertical and horizontal line scans through the center of the (00)-spots. This accounts for a possible sample tilt and potential asymmetries of the diffraction spots due to the presence of periodic surface steps or similar features known to cause deviations from a regular circular spot shape.<sup>19</sup>

An additional parameter used to evaluate the surface roughness of each sample was the average of the image root mean square (RMS) of AFM images of different locations around the sample's center that feature comparable resolution (Table II). Neglected here were features that on average occurred less than once per  $100\text{ nm} \times 100\text{ nm}$ , i.e., were uncommon within the transfer width of the SPA-LEED setup. This enabled the correlation between RMS and  $Q_{00}$ -factors and ensured that irregular features, often included in the images as points of reference, do not unduly influence the result.

The  $Q_{00}$ -factors and RMS values as well as types of topographies observed through AFM (Fig. 1) varied for each combination of  $T_g$  and  $T_a$ . The growth mode for all chosen growth parameters can be qualified as Stranski-Krastanov-like,<sup>19</sup> featuring varying degrees of 2D and 3D nucleation on top of a wetting layer. The wetting-layer thickness was not directly measured. However, through estimation

**TABLE II.** Growth and annealing temperature dependence of EuS film<sup>a</sup> roughness (RMS).

$T_g$	RMS (Å)		RMS (Å)		RMS (Å)	
	$T_a = 150\text{ }^\circ\text{C}$	Cat.	$T_a = 300\text{ }^\circ\text{C}$	Cat.	$T_a = 400\text{ }^\circ\text{C}$	Cat.
RT	4.9 (5)/5.4(5)	1/2	5.6(6)	2	4.4(5)	1
150 °C	-		7.5(7)	3	5.4(4)	2
300 °C	-		4.3(2)	1	9(1)	3
400 °C	-		-		4.4(2)	1

<sup>a</sup>All samples were deposited with a film thickness of 4 nm.

of the inelastic mean free path,<sup>22</sup> a complete covering of the substrates by a homogeneous EuS wetting layer with a thickness of approximately 2 nm or more can be inferred as no Auger signal of either substrate constituent was observed after EuS evaporation. Three categories of topography could be distinguished with only one sample ( $T_g = \text{RT}$ ,  $T_a = 150\text{ }^\circ\text{C}$ ) having shown more than one. The category assigned to each topography is indicated in both Tables I and II. The three categories are defined as follows:

**Category 1** topographies feature sporadic 3D nucleation (grains) with roughly circular base area on the wetting layer (Fig. 1(a), (d)). Grain coverages were below 2 % of the surface area for all such samples. Generally, increased coverage was observed for higher  $T_g$  and  $T_a$ . Due to the low grain coverage only the wetting layer contributed to the RMS values between 4.5 - 5 Å and comparatively low  $Q_{00}$ -factors. The individual mean heights of the observed grains ranged up to 80 nm. In the case of one sample ( $T_g = T_a = 400\text{ }^\circ\text{C}$ ), they were found to be linearly correlated with their base area [Fig. 2(a)] consistent with a thermally stable 3D growth mode featuring a constant ratio between surface and interface free energies.<sup>20</sup> For other category 1 samples, a similar correlation could not be established through graphical analysis because of the infrequency of grains on any given AFM image and the introduction of a rather sizeable relative error between grain parameters when attempting to combine results from different images due to differences in resolution, scanning speed and image processing.

**Category 2** topographies feature a high coverage (>50 %) of the wetting layer with 2D nuclei and sporadic occurrences of additional 3D nucleation. This category was observed exclusively for samples

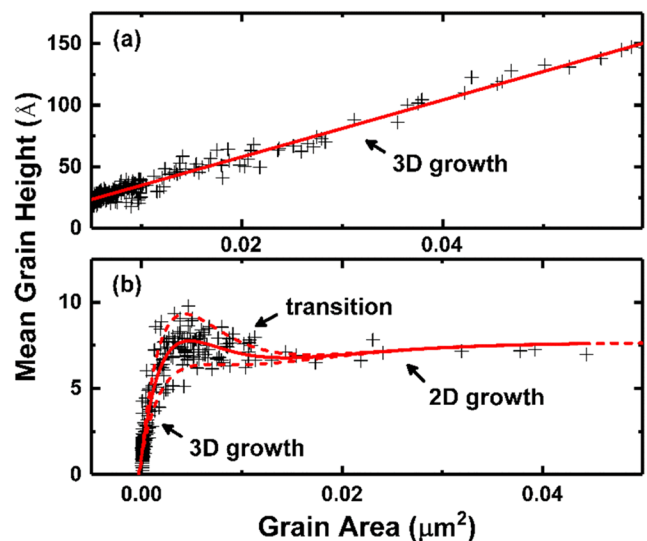


**FIG. 2.** Correlation between base area and mean heights of individual grains obtained through AFM investigation of two EuS thin films of 4 nm thickness on InAs(100). Grains were examined in (a) a  $20\text{ }\mu\text{m} \times 20\text{ }\mu\text{m}$  ( $T_g = T_a = 400\text{ }^\circ\text{C}$ ) and (b) a  $0.75\text{ }\mu\text{m} \times 1.5\text{ }\mu\text{m}$  area ( $T_g = 150\text{ }^\circ\text{C}$ ,  $T_a = 300\text{ }^\circ\text{C}$ ). (a) features a linear correlation (red fit), consistent with a stable 3D nucleation mode. (b) shows behavior consistent with a transition from 3D to 2D growth. Red solid line: fit of the equilibrium growth path using an empirical model [Eq. (1)]. Red dashed lines: thermodynamically valid growth paths with increased (upper) and decreased (lower) contribution of the 3D growth mode.

grown at RT and 150 °C with annealing temperatures up to 400 °C. The obtained RMS values of about 5.5 Å, account for both, the wetting layer and the 2D growth as well as their height difference. When considered in isolation, the feature RMS of the 2D growth was remarkably smooth, ranging from 2.5 - 3.7 Å, close to the expected level of the background noise. In correlation with the high coverage with smooth 2D features, that possess lateral dimensions well above the SPA-LEED transfer width, category 2 samples featured the highest quality factors ( $Q_{00} > 3$ ). Two examples of this category are shown in Fig. 1(a\*) and 1(b). Both featured 2D island growth (white arrows) with heights between 3 - 5 monolayers (ML). Here, we assumed that the  $Q_{00}$ -factors of the sample ( $T_g = RT$ ,  $T_a = 150$  °C) that showed both, category 1 and 2 topographies corresponded to the latter because the RMS of the observed wetting layer is comparable to other category 1 samples [see Figures 1(a) and (d)], while its  $Q_{00}$ -factor is significantly higher.

**Category 3** topographies feature a high frequency of 3D nucleation exceeding one feature per 100 nm × 100 nm. Consequently, the associated RMS values (7 - 10 Å) were the highest of all the categories while the  $Q_{00}$ -factors were comparatively low. An example of a category 3 topography is shown in Fig. 1(c). The surface of this particular sample ( $T_g = 150$  °C,  $T_a = 300$  °C) showed a high degree of grain coverage of 49(2) % evaluated over a total area of 14 μm × 14 μm. Figure 2(b) shows the relationship between the mean height and base area of individual grains observed in a 0.75 μm × 1.50 μm area representative of all recorded AFM images for this sample. Due to the high number of data points, it represents a histogram of the growth states and growth paths available for nucleation in the context of the thermodynamics of the system. The behavior of the data indicates three stages of growth. The initial stage, found for small grain areas  $A$  below 0.001 μm<sup>2</sup>, is defined by a steady increase in grain height with  $A$ . This is comparable to the linear behavior of the 3D growth mode shown in Fig. 2(a). The second stage is marked by a widening distribution of grain heights for increasing values of  $A$  followed by an eventual narrowing. This indicates an opening up of possible growth paths which subsequently converge again. The third stage, 2D nucleation, features a nearly constant height for grains featuring a grain area above 0.02 μm<sup>2</sup>.

The observed behavior suggests a thermodynamic competition between a 3D and a 2D growth mode,  $z_{3D}(A)$  and  $z_{2D}(A)$ , in which  $z_{3D}$  initially dominates before becoming thermodynamically unfavorable with increasing grain area  $A$ . In this model, the equilibrium growth path  $z_{eq}(A)$  for which the associated Gibbs free energy is minimized can be expressed by the following empirical relationship:

$$z_{eq}(A) = z_{3D}(A) \times \exp(-E \times A) + z_{2D}(A) + z_0 \\ = mA \times \exp(-E \times A) + z_{max} \times (1 - \exp(-d \times A)) + z_0. \quad (1)$$

Here,  $z_{3D}(A)$  is described by a linear relation with slope  $m$  that is proportional to the characteristic ratio between the surface and interface free energy.  $z_{2D}(A)$  is represented by a saturation function describing growth up to a characteristic grain height  $z_{max}$ . The receding contribution of the 3D growth mode is expressed by the additional Boltzmann factor  $\exp(-E \times A)$ , with  $E \propto \Delta G_{3D/2D}/k_B T$ , where  $\Delta G_{3D/2D}$  is the difference in Gibbs free energy per μm<sup>2</sup> between grains purely in the 3D and 2D growth mode. Applying this model to the data yields the fit (red solid line) in Fig. 2(b). The two additional

red dashed lines represent non-equilibrium growth paths defined by an increase (upper curve) and decrease (lower curve) by  $1/e$  of the contribution of  $z_{3D}(A)$  to the fit, respectively. They represent two of many possible growth paths with a sufficiently small difference in free energy  $\Delta G$  to  $z_{eq}(A)$  ( $\Delta G \approx k_B T$ ) to have a non-negligible likelihood of contributing to the observed distribution of growth states.

Due to all three curves reflecting the observed distribution of growth states reasonably well, the assumption of a competition between 3D and 2D growth as the source of the observed correlation between mean grain height and base area can be considered validated. It therefore stands to reason that topographies of category 3 are the result of hybrid growth modes between those leading to topographies of category 1 and 2.

Overall, category 2 topographies show the most potential for future application. While they featured slightly higher total RMS values than category 1 samples, the RMS of the 2D islands that were only observed for category 2 samples was exceptionally low. As the RMS values for category 2 samples were sensitive to both, wetting layer and 2D growth an increase in the surface coverage of the latter through optimization of the growth parameters is expected to yield lower total RMS values than observed up to now. Also, the resulting higher  $Q$ -factors of category 2 topographies suggest a more highly ordered surface in comparison to both, category 1 and 3 topographies. Hence, optimizing the growth parameters of category 2 samples will be a good starting point towards eventual layer-by-layer growth.

#### IV. CONCLUSION

The dependence of the surface quality of EuS films on InAs(100) on the growth and annealing temperatures  $T_g$  and  $T_a$  was investigated and confirmed using SPA-LEED and AFM. The films were determined to be epitaxial while the growth mode was identified as Stranski-Krastanov-like. The examined sample topographies were sorted into three categories defined by the varying degrees of observed 3D and 2D nucleation.

The most promising category for future application was observed for samples grown at RT and 150 °C with annealing temperatures up to 400 °C. It featured a high surface coverage with low RMS 2D island growth and a high quality factor.

Further attempts at optimization of the surface quality of EuS films on InAs are therefore recommended for growth parameters around  $T_g = RT/150$  °C and  $T_a = 400$  °C with the goal of increasing the coverage of the wetting layer with 2D islands and approaching layer-by-layer growth.

#### ACKNOWLEDGMENTS

The authors of this paper want to express their gratitude towards Professor Dr. Joachim Heberle and Emanuel Pfitzner for sharing their AFM setup and valuable time.

#### REFERENCES

- 1 S. A. Wolf *et al.*, *Science* **294**(5546), 1488–1495 (2001).
- 2 M. N. Baibich *et al.*, *Physical Review Letters* **61**(21), 2472 (1988).
- 3 R. A. Duine, K. J. Lee, S. S. Parkin, and M. D. Stiles, *Nature Physics* **1** (2018).
- 4 H. Yoda *et al.*, *2017 IEEE International Memory Workshop (IMW)*, IEEE, 2017.

- <sup>5</sup>V. Gaspare and F. Casoli, *Ultra-high-density magnetic recording: storage materials and media designs* (CRC Press, 2016).
- <sup>6</sup>P. Wachter, *C R C Critical Reviews in Solid State Sciences* **3**, 189–241 (1972).
- <sup>7</sup>P. Pouloupoulos *et al.*, *Applied Physics Letters* **100**, 211910 (2012).
- <sup>8</sup>S. Demokritov, U. Rucker, and P. Grünberg, *J. Magn. Magn. Mater.* **163**, 21–26 (1996).
- <sup>9</sup>W. Söllinger *et al.*, *Phys. Rev. B* **81**, 155213 (2010).
- <sup>10</sup>P. Fumagalli, J. Schirmeisen, and R. J. Gambino, *Phys. Rev. B* **57**, 14294–14298 (1998).
- <sup>11</sup>S. D. Pappas *et al.*, *Sci. Rep.* **3**, 1333 (2013).
- <sup>12</sup>P. Pouloupoulos *et al.*, *Appl. Phys. Lett.* **104**, 112411 (2014).
- <sup>13</sup>A. Goschew, M. Scott, and P. Fumagalli, *Appl. Phys. Lett.* **109**, 062401 (2016).
- <sup>14</sup>W. Zinn, B. Saftic, N. Rasula, M. Mirabal, and J. Köhne, *J. Magn. Magn. Mater.* **35**, 329–336 (1983).
- <sup>15</sup>C. J. P. Smits *et al.*, *J. Appl. Phys.* **95**, 7405 (2004).
- <sup>16</sup>S. Senba *et al.*, *J. Korean Phys. Soc.* **62**, 2109–2112 (2013).
- <sup>17</sup>A. Goschew, J. Griesmar, and P. Fumagalli, *Thin Solid Films* **625**, 106–110 (2017).
- <sup>18</sup>U. Scheithauer, G. Meyer, and M. Henzler, *Surface Science* **178**(1-3), 441–451 (1986).
- <sup>19</sup>H. Lüth, *Solid surfaces, interfaces and thin films* (Springer, Berlin, 2001), Vol. 4, pp. 67–108.
- <sup>20</sup>V. Dubrovskii, *Nucleation Theory and Growth of Nanostructures* (Springer, Berlin, Heidelberg, 2014), pp. 38–43.
- <sup>21</sup>J. Wang, Ph.D. thesis, Mathematisch-Naturwissenschaftlich-Technischen Fakultät der Martin-Luther-Universität Halle-Wittenberg, 2005.
- <sup>22</sup>S. Tanuma, C. J. Powell, and D. R. Penn, *Surf. Interface Anal.* **11**, 577 (1988).